# The Solvation Structure of Mg Ions in Dichloro Complex Solutions from First-Principles Molecular Dynamics and Simulated X-ray Absorption Spectra

Liwen F. Wan* and David Prendergast

Joint Center for Energy Storage Research (JCESR), The Molecular Foundry, Lawrence Berkeley National Laboratory, Berkeley, California 94720, United States

Ⓢ *Supporting Information*

**ABSTRACT:** The knowledge of Mg solvation structure in the electrolyte is requisite to understand the transport behavior of Mg ions and their dissolution/deposition mechanism at electrolyte/electrode interfaces. In the first established rechargeable Mg-ion battery system [D. Aurbach et al. *Nature* **2000**, *407*, 724], the electrolyte is of the dichloro complex (DCC) solution family, Mg-$(AlCl_2BuEt)_2$/THF, resulting from the reaction of $Bu_2Mg$ and $EtAlCl_2$ with a molar ratio of 1:2. There is disagreement in the literature regarding the exact solvation structure of Mg ions in such solutions, i.e., whether $Mg^{2+}$ is tetra- or hexacoordinated by a combination of $Cl^-$ and THF. In this work, theoretical insight into the solvation complexes present is provided based on first-principles molecular dynamics simulations (FPMD). Both Mg monomer and dimer structures are considered in both neutral and positively charged states. We found that, at room temperature, the $Mg^{2+}$ ion tends to be tetracoordinated in the THF solution phase instead of hexacoordinated, which is the predominant solid-phase coordination. Simulating the X-ray absorption spectra (XAS) at the Mg K-edge by sampling our FPMD trajectories, our predicted solvation structure can be readily compared with experimental measurements. It is found that when changing from tetra- to hexacoordination, the onset of X-ray absorption should exhibit at least a 1 eV blue shift. We propose that this energy shift can be used to monitor changes in the Mg solvation sphere as it migrates through the electrolyte to electrolyte/electrode interfaces and to elucidate the mechanism of Mg dissolution/deposition.
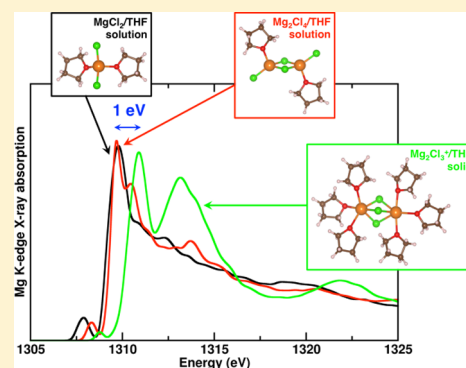
## INTRODUCTION

There is a growing need to develop new energy storage systems that can serve as competitive alternatives to current Li-ion technologies, but which are much safer and less expensive. One approach is to develop multivalent ion batteries that can, on one hand, double or triple the specific capacity by incorporating divalent or trivalent ions. For example, the theoretical volumetric capacity of Mg-ion batteries can reach 3833 mAh/$cm^3$, compared to 2046 mAh/$cm^3$ of the monovalent Li-ion batteries.[1] On the other hand, the energy density can also be increased, since it is defined as the product of unit charge per conducting ion and the cell voltage. However, in reality, the cell voltage is often hindered by the difficulties of developing high-voltage cathode materials that allow for fast and reversible intercalation.[1−5] This is purported to be mainly due to the strong electrostatic interactions between the multivalent ions and their surroundings that hinder ion transport kinetics.

The first established rechargeable multivalent battery is based on the Mg ion, developed by Aurbach et al. in 2000.[6] The cathode and anode are chosen to be Chevrel phase $Mo_6S_8$ and Mg metal, respectively, which are then separated by an electrolyte comprising Mg organohaloaluminate (Mg-$(AlCl_2BuEt)_2$) salts in tetrahydrofuran (THF) solution, the dichloro complex (DCC) solution. Depending on the initial ratio of the $Bu_2Mg$ and $EtAlCl_2$ reagents, a variety of complex species, such as $MgCl^+$, $MgCl_2$, $Mg_2Cl_3^+$, $AlEt_3$, $Et_2AlCl_2^+$, $Et_2AlCl$, etc., can be formed in the THF solution.[1,7] One critical aspect to understand the working mechanism of this Mg battery cell is to identify the active chemical species that carries Mg ions through the electrolyte and thereafter determine Mg deposition/dissolution energetics at electrolyte/electrode interfaces.

It is generally recognized that Mg ions are strongly coordinated in DCC solutions by a combination of inorganic counterions, $Cl^-$, and organic solvent, THF, ligands. However, the exact solvation structure of the Mg ion is still not clear. Using Raman spectroscopy,[8] a transmetalation process is identified between the $R_2Mg$ and $AlCl_{3−n}R_n$ reagents, where R is an alkyl or aryl functional group. As a result, the electrolyte solution will contain Mg dications bound to $Cl^-$ and Al that adopts all the organic R groups and any remaining $Cl^-$. In the meantime, the Mg and Al complex salts will interact with THF molecules to form bulky solvation spheres. The structures of these solvation spheres have been interrogated using multinuclear magnetic resonance (NMR) on solution phases and X-
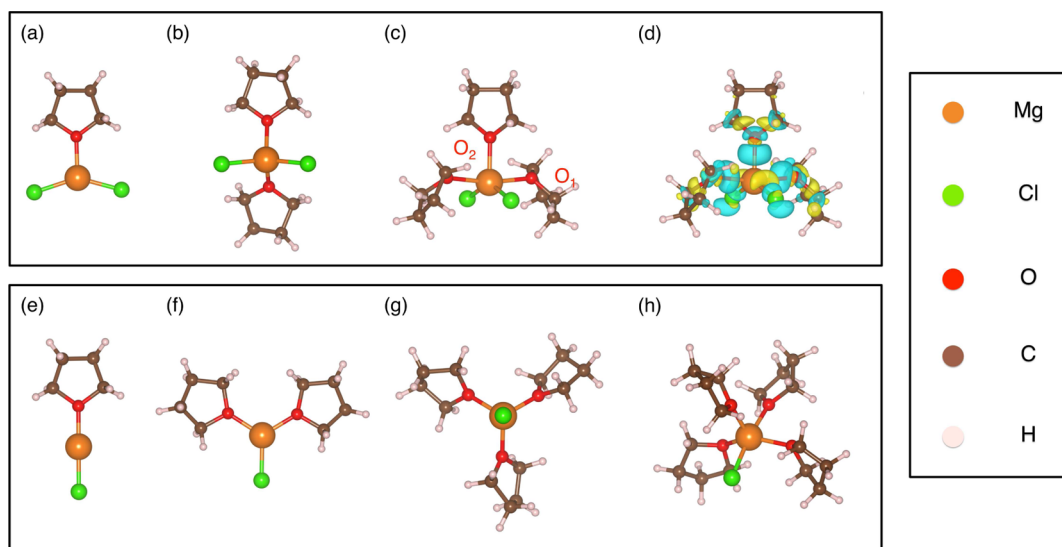
**Figure 1.** DFT-PBE optimized solvation structures for $MgCl_2$ (a–c) and $MgCl^+$ (e–h) monomers in THF. (d) Charge renormalization due to bonding for the $MgCl_2 \cdot 3THF$ structure, where cyan and yellow represents negative and positive charge densities. The Mg, Cl, O, and H atoms are shown in orange, green, red, and off-white, respectively. The same color nomenclature is also used in the rest of the structural representations.

ray diffraction (XRD) techniques for recrystallized samples, with the conclusion that the Mg ion is believed to be hexacoordinated in either monomers or dimers.[1,9,10] However, the Mg-based NMR evidence for hexacoordination is merely inferred by comparison with a reference solution assumed to also be hexacoordinated.[11] The case for hexacoordination is further supported by Benmayza et al.,[12] using Mg K-edge X-ray absorption spectroscopy. By comparing the Mg K-edge near-edge X-ray absorption fine structure (NEXAFS) of the electrolyte and a recrystallized $[Mg_2Cl_3 \cdot 6THF]^+(AlCl_4)^-$ sample, determined by XRD to exhibit hexacoordinated Mg ions, similarities in spectral line shape and absorption onset energies are observed in both cases, and thus the same coordination structure of Mg ions is deduced. In contradiction of the predominant hexacoordination viewpoint, Nakayama et al. determined that Mg ions should be tetracoordinated in the DCC solutions based both on NEXAFS and Fourier transformed extended X-ray absorption fine structure (EXAFS) spectra in addition to NMR measurements.[7] The purpose of this work is not only to resolve this apparent lack of agreement in the literature about the solvation structure of Mg ion in dichloro solutions but also to provide valuable information on the local electronic structures and energetics of the solvated $Mg^{2+}$ ions.

In addition to the prototype DCC solutions, other electrolytes have also been synthesized that involve the formation of $MgCl_x \cdot nTHF$. For example, non-Grignard solutions, such as the magnesium aluminum chloro complex (MACC) in THF, have been developed in recent years as "simple and cheap" alternatives to DCC. A general understanding of how $MgCl_x$ is solvated in THF is also beneficial to understand ion transport and dissolution/deposition in MACC.

In this study, we use first-principles methods to examine the solvation structure of the Mg dication as it interacts with the $Cl^-$ anions and THF molecules. Initially, we use density functional theory (DFT) to predict the formation energies and local geometries of Mg-coordinating clusters in the absence of finite temperature effects. Armed with this insight, we use first-principles molecular dynamics (FPMD) simulations to obtain the equilibrium solvation structure in THF at room temper-

ature. The Mg K-edge NEXAFS and EXAFS spectra are then calculated based on the solvation structures we obtained from the molecular dynamics (MD) configurational sampling. This is believed to be a reliable approach to interpret XAS spectra from electronic structure calculations.[13−15] Finally, the obtained XAS spectra are compared with existing experimental measurements.

## ■ METHODS

Within the framework of DFT,[16] the electronic structure calculations are performed using the Vienna Ab initio Simulation Package (VASP).[17,18] The Perdew−Burke−Ernzerhof (PBE) formulation of the generalized-gradient approximation (GGA) is used to approximate the exchange-correlation functional.[19] The all-electron ion potentials are replaced by much shallower projector-augmented wave potentials.[20,21] A 400 eV energy cutoff is used to truncate the plane-wave basis set, and only the $\Gamma$-point ($\mathbf{k} = 0$) is sampled for the Brillouin zone integration. Although long-range van der Waals dispersion forces may play a role in determining the nonbonding intermolecular interactions, their inclusion has negligible impact on the intramolecular bonding between Mg and its ligands, as shown in the Supporting Information. Therefore, the corrections for van der Waals dispersion forces are excluded throughout our investigation.

Gas-phase structures are first simulated using the static DFT approach. One solvated Mg cluster is placed in a $30 \times 30 \times 30$ Å or $40 \times 40 \times 40$ Å simulation box depending on the specific size of the molecules. The structure is considered as fully optimized if the residual atomic forces are smaller than 10 meV/Å. The solvation structures in the liquid phase are realized by performing FPMD simulations. For the monomers, one $MgCl_2$ or $MgCl^+$ is implanted with 55 THF molecules in a $19.5 \times 19.5 \times 19.5$ Å simulation box. The resulting Mg salt concentration is approximately 0.22 M, which is close to that of the experimental electrolyte studied by Nakayama et al.[7] (0.25 M) and approximately half that of Benmayza et al.[12] (0.4 M). For the case of the dimers, i.e., $Mg_2Cl_4$, $Mg_2Cl_3^+$, the same simulation cell is used, and the resulting salt concentration is doubled. However, with respect to studying the evolution of various Mg-containing species and the potential formation of complex oligomers, these simulations are more representative of dilute solutions, since each supercell initially contains only one solute (monomer or dimer) and hence true solute−solute interactions are absent, although dimer dissociation is possible. All the FPMD simulations are equilibrated at 300 K using a Nosé thermostat.[22] A time step of 0.25 fs is used, and the systems typically reach equilibration within 5 ps.

**Table 1. DFT-PBE Formation Energies and Structural Parameters for the Molecular Structures Presented in Figure 1**

| molecular structure | formation energy[a] (eV) | formation energy per THF (eV) | Mg−O bond length (Å) | Mg−Cl bond length (Å) |
|---|---|---|---|---|
| $MgCl_2 \cdot 1THF$ | −1.15 | −1.15 | 2.03 | 2.23 |
| $MgCl_2 \cdot 2THF$ | −2.04 | −1.02 | 2.07 | 2.28 |
| $MgCl_2 \cdot 3THF$ | −2.36 | −0.79 | 2.23/2.09[b] | 2.32 |
| $MgCl^+ \cdot 1THF$ | −2.90 | −2.90 | 1.93 | 2.14 |
| $MgCl^+ \cdot 2THF$ | −4.87 | −2.44 | 1.97 | 2.18 |
| $MgCl^+ \cdot 3THF$ | −6.29 | −2.10 | 2.02 | 2.23 |
| $MgCl^+ \cdot 4THF$ | −6.79 | −1.70 | 2.11 | 2.32 |

[a]The cluster formation energy is defined as $E_{form} = E_{tot} - E_{MgCl_2/MgCl^+} - n \cdot E_{THF}$. [b]Bond length for $Mg-O_1$ and $Mg-O_2$, respectively, as marked in Figure 1c.

The NEXAFS calculations are conducted using the PWscf code in the QuantumESPRESSO software package with the Shirley reduced basis set for efficient Brillouin zone (**k**-point) sampling.[23,24] Ultrasoft pseudopotentials are used for all elements, and for the excited atom, i.e. Mg, a modified pseudopotential is used with one electron removed from the 1s core orbital.[25] Within the excited electron and core-hole (XCH) approximation, as thoroughly discussed in ref 26, the first core-excited state is approximated within constrained-occupancy DFT by inclusion of both the core-hole pseudopotential and the excited electron (placed at the conduction band minimum) in the definition of the self-consistent electron density, while the higher energy excitations are obtained from non-self-consistent-field calculations for the unoccupied density of states. Following Fermi's golden rule, the transition probabilities at each energy are calculated and convoluted with a uniform Gaussian broadening of 0.2 eV. It has been established previously that an appropriate alignment scheme needs to be applied to all calculated spectra so that the onset energies can be compared.[27] In this work, we align the calculated spectrum of rocksalt MgO with experiment and use the same constant to shift all of our calculated Mg K-edge spectra for the Mg ions in THF solution. In addition, EXAFS spectra are obtained using the FEFF8 code, where the scattering phase shifts are calculated self-consistently.[28]

## RESULTS AND DISCUSSIONS

**$MgCl_2$ and $MgCl^+$ Monomers.** Within PBE-GGA, the zero temperature molecular structures of Mg monomers are studied using the static cluster model. The optimized structures for each solvation shell are shown in Figure 1, and the detailed structural parameters are summarized in Table 1. For both neutral and charged monomers, the Mg ion can accommodate up to 5 ligands, while hexacoordinated initial structures relax by shedding one or more THF molecules from the inner solvation shell. For the charge neutral monomer $MgCl_2$, the linear Cl−Mg−Cl bond starts to bend as THF molecules approach the Mg ion. Depending on the number of THFs, the bond angle varies from 146° ($MgCl_2 \cdot 1THF$) to 133° ($MgCl_2 \cdot 2THF$). This is mainly due to the electrostatic repulsion between electrons in Cl 3p orbitals and oxygen lone pairs from THF. In addition, when $MgCl_2$ is surrounded by a large number of THFs, the steric repulsion between the THF molecules in such close proximity makes it difficult to fit many in the first solvation shell. For example, in Figure 1c, there are two types of Mg−O interactions in this 5-fold coordination structure. The two side THFs are related by symmetry, and their Mg−O distance is 2.23 Å, which is much longer than typical Mg−O distances, which are in the range 1.9−2.1 Å. Therefore, a weaker binding strength should be expected between the Mg ion and these two THF molecules. As we can see from Table 1, the cluster formation energy increases by only 0.3 eV compared to the 4-fold coordination case. This small energy gain can be overcome by finite temperature effects (both enthalpic and entropic), as we will discuss later in this section. It should be noted here that

the 6-fold coordination structure, as proposed in ref 1 and assumed by many other groups (most likely based on the prevalence of 6-fold coordination in Mg crystals and aqueous solution), is found to be energetically unstable even within our static cluster models. The energy cost to preserve such octahedral coordination can range from 0.6 to 4.3 eV depending on the specific DFT optimization scheme. Using a typical classical force field, such as the optimized potentials for liquid simulations (OPLS) force field, also fails to reproduce our PBE solvation structure of the Mg ion and instead results in 6-fold coordination. A detailed discussion of the results obtained using different simulation methods can be found in the Supporting Information of this article.

For the positively charged $MgCl^+$, the static cluster model formation energy (our zero-temperature, gas-phase approximation to the solvation energy) is considerably larger than that of neutral $MgCl_2$. This is due to the strong electrostatic interactions between the charged $MgCl^+$ unit and the electronegative O on the THFs. In contrast to the structure presented in Figure 1c, the THF molecules in the $MgCl^+ \cdot nTHF$ solvation shell are always equally distributed in space. The resulting Mg−O bond length is approximately the same for all Mg-THF pairs, although for large $n$, e.g., $MgCl^+ \cdot 4THF$, the Mg−O bond length is again longer than typical Mg−O bonds.

In Figure 1d, the bonding charge density, rendered as the charge density difference between the solvated cluster and its individual components, is presented for the $MgCl_2 \cdot 3THF$ structure. The cyan and yellow color represents negative and positive charge accumulation due to bonding. A typical ionic bonding between Mg and O or Cl p states is observed. From Table 1, the energy cost to strip THF away from Mg is at least 0.8 eV. The interaction between $Mg^{2+}$ and $Cl^-$ is much stronger. For example, the PBE estimate of the dissociation energy of Cl from the $MgCl_2 \cdot 3THF$ molecule is 3.4 eV. This is comparable with the dissociation energy of one Cl from the $MgCl_2$ molecule at 0 K, which is about 4.1 eV. The strong ionic bonding characteristic can also be verified by plotting the partial density of states for specific atomic orbitals. As shown in Figure 2, only minor hybridization is found between the Mg s states and Cl or O p states at about 2 eV below the highest occupied molecular orbital (HOMO). The corresponding charge density is presented in the red box in Figure 2, where a slight overlap between the Mg 3s orbital and Cl 3p orbital is observed.

Using simple cluster models, the formation energies we obtained in Table 1 should be referred to as formation enthalpies at zero temperature. However, at finite temperature, this enthalpic term is likely to be revised, and the entropic contribution to the solvation free energy may become significant, resulting in altered Mg solvation structures. Here, we perform FPMD simulation to study the room temperature
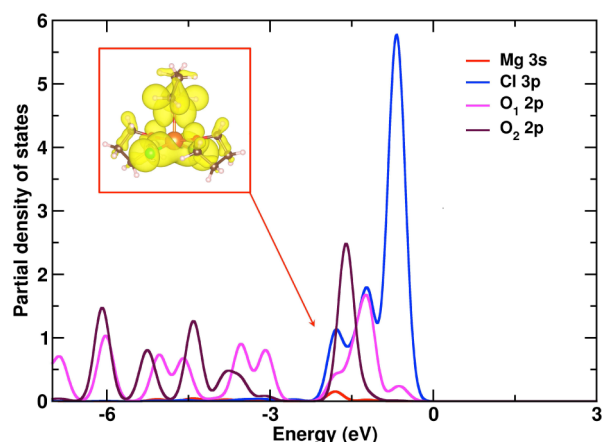
**Figure 2.** Partial density of states for the MgCl$_2$·3THF molecule based on DFT-PBE. The localized charge density is calculated and plotted at 2 eV below the HOMO, which is arbitrarily aligned with zero on the energy axis.

behavior of MgCl$_2$ within THF solutions in the dilute limit. We initialize our MD simulation by placing one hexacoordinated MgCl$_2$·4THF unit (Figure S2b) in the THF solution. After 0.4 ps, two THF molecules leave the first solvation shell, and the Mg ion becomes tetracoordinated. Upon equilibration, this tetracoordinated structure remains, and a snapshot of the equilibrated MgCl$_2$·2THF structure is given in Figure 3 (top). The radial distribution function (RDF) is calculated and averaged for 5 ps after equilibration and plotted in Figure 3 (top). The average bond length for Mg–Cl is approximately 2.3 Å, which is approximately the same as our simple cluster models. The RDF peak for the Mg–O pair is slightly broadened, indicating dynamical fluctuations in the weaker coordination of Mg ions by THF molecules. Compared to our isolated cluster models, the Mg coordination number is reduced from 5 to 4 due to the impact of finite temperature. The

dynamical behavior of the charged MgCl$^+$ monomer is fundamentally similar to its neutral counterpart. The total coordination number remains at 4, but in this case the ligands comprise one Cl$^-$ and three THFs as shown in Figure 3 (bottom).

**Mg$_2$Cl$_4$ and Mg$_2$Cl$_3^+$ Dimers.** It has been proposed in the literature that complex (MgCl$_2$)$_x$/THF structures can be developed by varying the molar ratio of MgCl$_2$ and THF. For example, crystalline morphology has been observed in the (MgCl$_2$)$_x$/THF complex solutions where the Mg ion tends to form large oligomers.[29] However, in battery electrolytes, the average salt concentration is usually lower than 1 mol/L. Therefore, if one excludes the possibility of large fluctuations in local concentration, only small molecules are expected to form, such as monomers or dimers. Unlike the simple structure of monomers, the dimer structures are usually complicated by their local symmetries. A nice summary of the possible dimer configurations of MgCl$_2$ can be found in ref 30. Based on the empirical polarized-ion model, it is proposed that the Mg dimers with $D_{2h}$ (Figure 4a) and $C_{3v}$ (Figure 4d) symmetries are energetically most stable. Within PBE-GGA, we find that the $D_{2h}$ symmetry possesses lower dimerization energy for the neutral state, while the situation is reversed for the charged state as shown in Table 2. Although the $D_{2h}$ and $C_{3v}$ clusters have different symmetries, the resulting charge for each ion is approximately the same as shown in Figure 4a,d. Based on these low-energy dimer configurations, their interactions with THF molecules are studied at zero temperature using cluster models. It is found that neither Mg$_2$Cl$_4$ ($D_{2h}$) nor Mg$_2$Cl$_3^+$ ($C_{3v}$) can incorporate more than 4 THFs in the first solvation shell.

By examining the PBE dimerization energies in Table 2, we notice the energy difference between the $D_{2h}$ and $C_{3v}$ symmetry for the charged Mg$_2$Cl$_3^+$ dimer is only ~0.3 eV. This small energy difference can be further lowered by increasing the number density of neighboring THFs. For example, in Figure
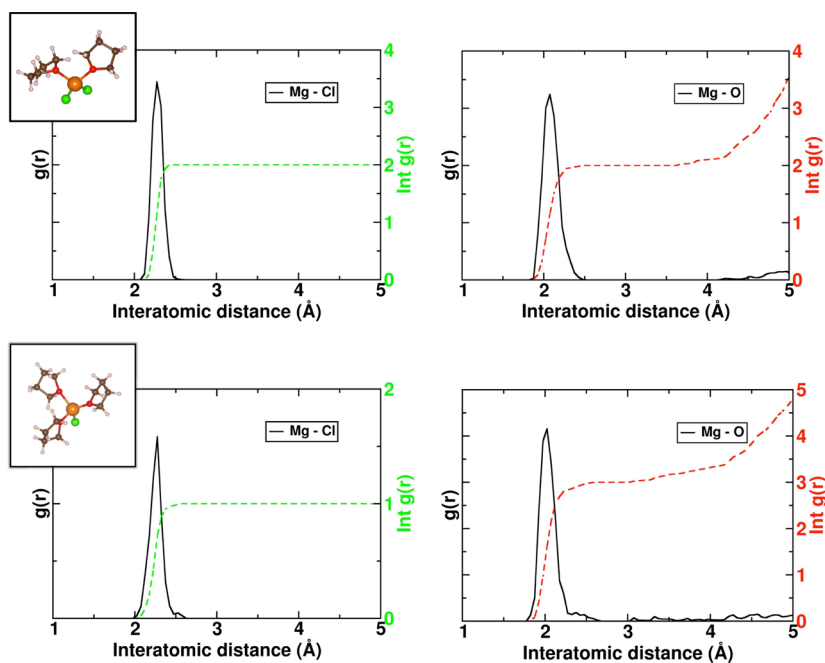


**Figure 3.** A representative molecular structure of MgCl$_2$·2THF (top) and MgCl$^+$·3THF (bottom) sampled from equilibrated FPMD simulations. The corresponding radial distribution functions and associated integrals for Mg–Cl (left) and Mg–O (right) atomic pairs are also presented.
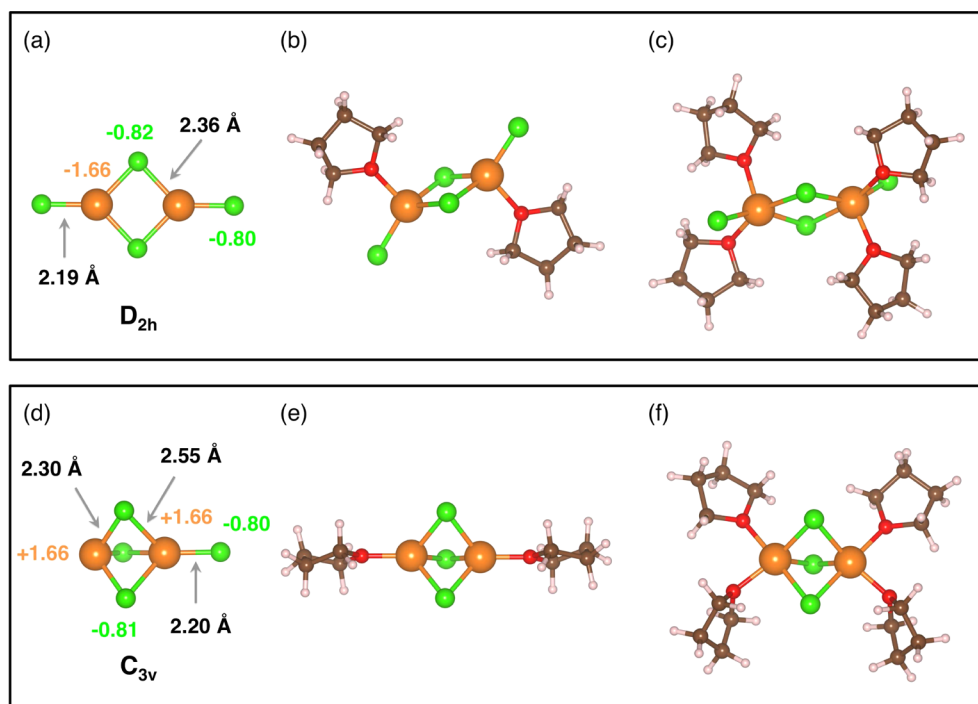
**Figure 4.** DFT-PBE optimized solvation structures for $Mg_2Cl_4$ and $Mg_2Cl_3^+$ dimers.

**Table 2. DFT-PBE Estimates of the Dimerization and Cluster Formation Energies for Selected Dimer Configurations**

| symmetry | molecular structure | dimerization energy[a] (eV) | formation energy[b] (eV) | formation energy per THF (eV) |
|---|---|---|---|---|
| $D_{2h}$ | $Mg_2Cl_4$ | −1.67 | − | − |
| | $Mg_2Cl_3^+$ | −2.29 | − | − |
| | $Mg_2Cl_4 \cdot 2THF$ | − | −2.17 | −1.08 |
| | $Mg_2Cl_4 \cdot 4THF$ | − | −2.92 | −0.73 |
| $C_{3v}$ | $Mg_2Cl_4$ | −1.13 | − | − |
| | $Mg_2Cl_3^+$ | −2.63 | − | − |
| | $Mg_2Cl_3^+ \cdot 2THF$ | − | −4.30 | −2.15 |
| | $Mg_2Cl_3^+ \cdot 4THF$ | − | −6.24 | −1.56 |

[a]The dimerization energy is defined as $E_{dim} = E_{tot} - 2E_{MgCl_2}$ or $E_{tot} - E_{MgCl_2} - E_{MgCl^+}$. [b]The cluster formation energy is defined as $E_{form} = E_{tot} - E_{Mg_2Cl_4/Mg_2Cl_3^+} - n \cdot E_{THF}$.

6a,b, the energy difference is reduced to as low as 0.035 eV. One can imagine that this energy may be easily overwhelmed at room temperature (0.026 eV thermal energy), where we find that the $Mg_2Cl_3^+$ $D_{2h}$ dimer configuration predominates. Indeed, upon placing the $C_{3v}$ dimer in THF solution at 300K, we observe that one of the center Mg−Cl bonds quickly breaks (within 0.2 ps), and an approximate $D_{2h}$-like symmetry results. From Figure 5b, we find that the breaking of $C_{3v}$ symmetry is irreversible and that our equilibrated configurations exhibit the approximate $D_{2h}$-like symmetry. The RDF is again averaged for 5 ps after equilibration and plotted at the bottom of Figure 5. Here the RDF plot for Mg−Cl pairs is decomposed into the individual contribution of Mg−Cl bonds at the center of the cluster (i.e., bridging Mg ions) or at the edge (coordinating only one Mg ion). The bond length distribution of the single Mg−Cl bond at the edge, shown in black, remains very sharp over time. However, the bond length distribution between Mg ions and the center Cl anions is much broader, which indicates stronger thermal fluctuations for these weaker bonds. Unlike the strictly 4-fold coordinated monomers, the Mg ion in the dimer structure can be either 4- or 5-fold coordinated depending on the local coordination number of Cl anions. It

is not, in fact, surprising to have this 5-fold coordination structure because the Mg ion prefers to be hexacoordinated by multiple counterions, as in the $MgCl_2$ crystal structure.

For the charge neutral $Mg_2Cl_4$ dimer, the $D_{2h}$ symmetry structure is more stable than that of $C_{3v}$ symmetry. For example, the optimization of an $Mg_2Cl_4 \cdot 5THF$ $C_{3v}$ configuration ultimately resembles a $D_{2h}$ symmetry structure, as one of the bridging Mg−Cl bonds breaks during optimization. Both structural configurations are given in Figure 6c,d. Similar behavior is also observed at room temperature with each Mg ion maintaining a tetracoordinated geometry with only two bridging Cl anions defining the dimer.

**Mg K-Edge X-ray Absorption Spectra Simulations.** To directly link to experimental evidence for Mg-coordination in DCC solutions, Mg K-edge NEXAFS spectra are simulated for different solvation configurations. In our calculations, we sample individual core-excited Mg atoms across the ensemble provided by our finite temperature MD simulations. The NEXAFS spectra, presented in Figure 7, are averages based on combining simulated spectra of at least 15 structures (well-separated in time along our MD trajectories) in each of the solvation scenarios considered. For the tetracoordinated $MgCl_2$
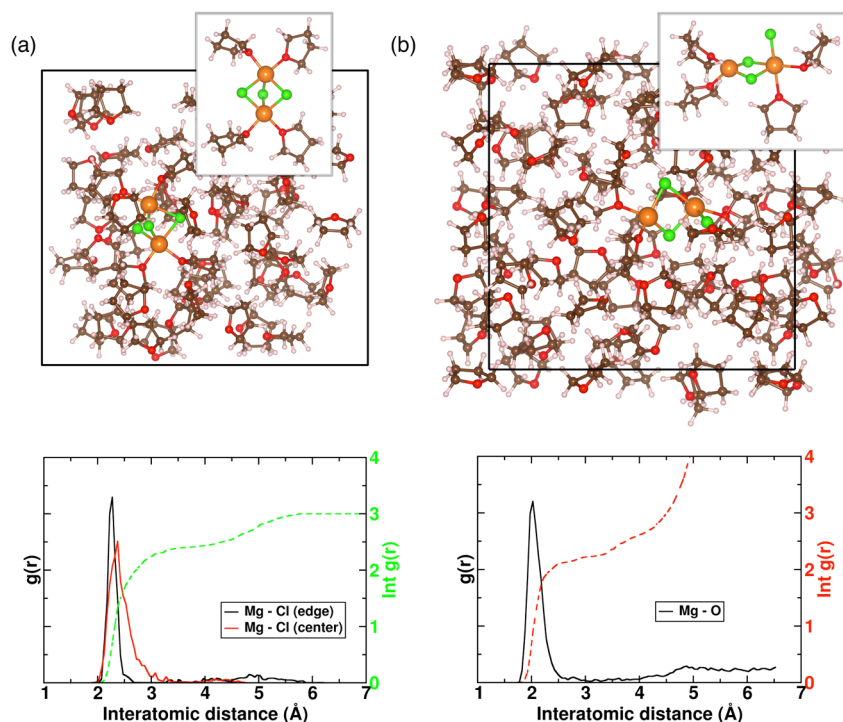
**Figure 5.** Representative FPMD snapshots of solvated $Mg_2Cl_3^+$/THF structures (top) and the sampled radial distribution functions (bottom) for (a) the initial $C_{3v}$ structure embedded in THF and (b) the equilibrated $D_{2h}$-like structure (see text for details). Insets are the enlarged molecular structures of $Mg_2Cl_3^+ \cdot 4THF$.
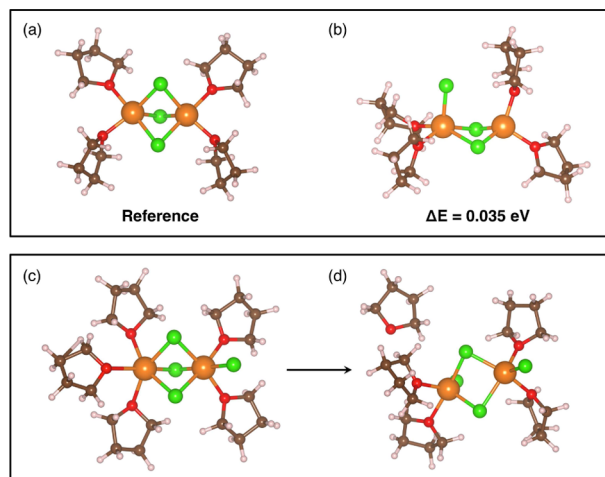


**Figure 6.** DFT-PBE optimized solvation structures for $Mg_2Cl_3^+ \cdot 4THF$ in approximate (a) $C_{3v}$ and (b) $D_{2h}$ symmetry and $Mg_2Cl_4 \cdot 5THF$ in approximate (c) $C_{3v}$ and (d) $D_{2h}$ symmetry.

and $Mg_2Cl_4$ solvation structures, the main-edge is observed at 1309.8 eV using the energy alignment scheme discussed above. One would expect the lowest-energy core-excited state of a Mg dication to be predominantly representative of $1s \rightarrow 3s$ transitions, which are dipole-forbidden. However, the instantaneously imperfect symmetry around the Mg ion at finite temperature can readily induce a first moment in the excited electron probability density, which will result in a weakly dipole-allowed transition. This phenomenon has been extensively explored for Li compounds[13] and is also evident in other Mg K-edge XAS studies of $CO_2$ adsorption in metal organic frameworks.[31] So, as expected, a pre-edge feature is evident in both solvation scenarios due to the thermal fluctuations of the

Mg−Cl and Mg−O coordination at room temperature. Only a few discrete excited states contribute to this pre-edge peak, and they are highly localized on the Mg-containing species. Taking the $MgCl_2 \cdot 2THF$ species as an example, the core-excited state electron density for the pre-edge and main-edge energies are exhibited in Figure 7a. The low-energy states are confined on the $MgCl_2 \cdot 2THF$ molecule, whereas the higher-energy states are more diffuse and extend to the neighboring THFs.

It is identified in ref 12 that the Mg ion is hexacoordinated in solid phases resulting from recrystallization of a DCC solution, forming a crystal structure with the formula $[Mg_2Cl_3 \cdot 6THF]^+(AlCl_3Et)$. For comparison with experiment, we perform a first-principles MD simulation of this solid structure at 300 K. It is found that the solvation shell of the Mg ion remains in the coordination geometry of $[Mg_2Cl_3 \cdot 6THF]^+$, as shown in Figure S5. In other words, the Mg ion maintains a 6-fold coordination with 3 $Cl^-$ and 3 THFs, although large fluctuations of Mg−Cl and Mg−O distances are observed. The RDF plots, comparing the experimentally measured XRD and MD simulated $[Mg_2Cl_3 \cdot 6THF]^+(AlCl_3Et)$ structures, are also given in the Supporting Information of this article. The corresponding Mg K-edge NEXAFS shows a 1 eV blue shift with respect to the solvated species, and in addition, a new broad peak appears at 1313.2 eV. This is analogous to the Mg K-edge spectra of other octahedral Mg compounds, such as MgO,[31,32] which display a similar onset energy but have their second peak at differing energies related to different bond lengths between cation and anions. Intuitively, the energy shift can be explained from two aspects: first, the change of residual charges on the excited atom and second, the increase of surrounding ligand field strength. For instance, moving from Mg metal to $MgCl_2$ solid, the local charge on Mg changes (nominally) from 0 to +2 and the corresponding first absorption peak at the Mg K-edge shifts from 1306 to 1311
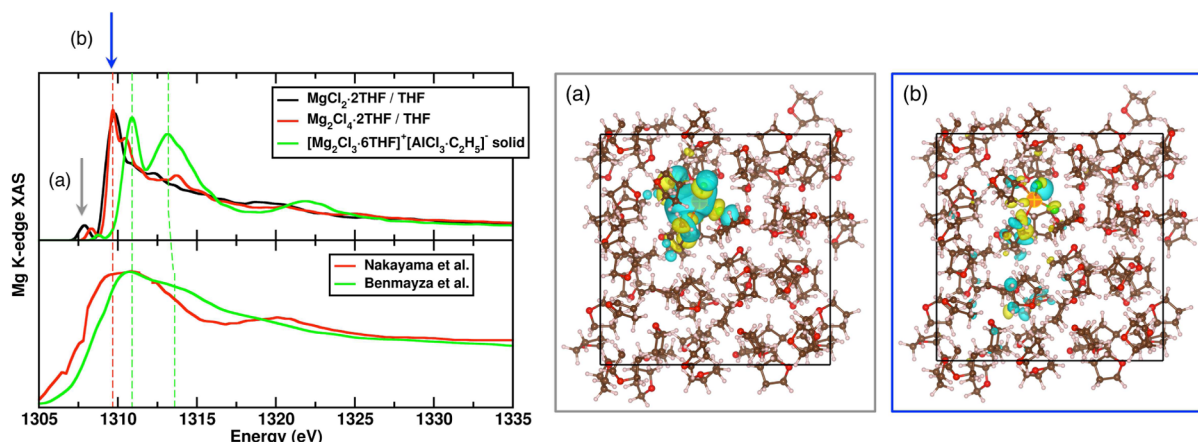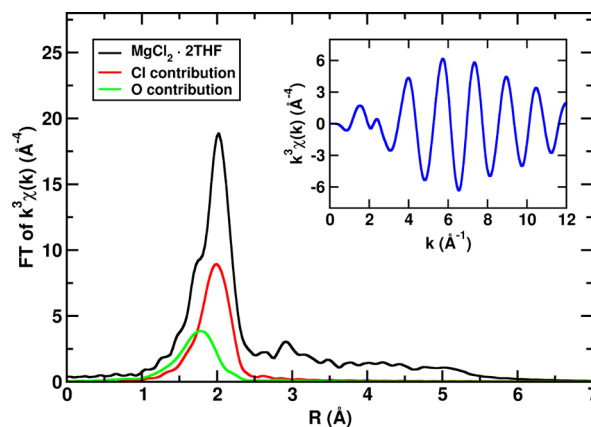
**Figure 7.** Calculated Mg K-edge NEXAFS spectra for $MgCl_2$/THF solution, $Mg_2Cl_4$/THF solution, and $[Mg_2Cl_3 \cdot 6THF]^+(AlCl_3 \cdot C_2H_5)$ crystal with comparison of the existing Mg K-edge measurements.[7,12] For the case of $MgCl_2$/THF, the wave function associated with the pre-edge and main-edge excited states are presented as isosurfaces at isovalue = 0.0004 $e/au^3$. The black box indicates the periodic boundary condition.

eV.[33] In this study, the Bader charge associated with the Mg atom stays almost constant, i.e., +1.73, +1.72, and +1.75 for $MgCl_2$ monomer, $Mg_2Cl_4$ dimer, and $[Mg_2Cl_3 \cdot 6THF]^+$ solid, respectively. However, the Mg-ligand coordination symmetry switches from tetrahedral to octahedral, which pushes the conduction band minimum or LUMO to higher energies resulting in a blue shift in the X-ray absorption onset.

From the literature, two experimental Mg K-edge NEXAFS measurements are available for the DCC solution,[7,12] which are both reproduced in Figure 7 to aid better comparison. In 2008, Nakayama et al. measured the Mg K-edge spectrum for bulk $Mg(AlCl_2EtBu)_2$/THF electrolyte and found a main-edge energy of 1309.5 eV.[7] By Fourier transforming the EXAFS spectrum and comparing with known hexacoordinated compounds, it is concluded that the Mg ion is tetracoordinated within the solution. In this study, the main-edge energies for our 4-fold coordinated models (Figure 7a,b) reside approximately at 1309.8 eV, which agree well with Nakayama's NEXAFS measurements, despite the lower-energy resolution of their measurement. In addition, we also simulated the EXAFS for the tetracoordinated Mg ions sampled from our FPMD trajectories, as presented in Figure 3. The obtained spectrum in Figure 8 is based on an average over 15 snapshots, the same used to calculate the NEXAFS spectrum. The Fourier transformation of the $k^3$ weighted $\chi(k)$ shows a main feature at $R = 2$ Å, which again matches with Nakayama's measurement for the Mg tetrahedral dimer, $(Mg_2Cl_2THF_4)^{2+}$. To further decompose the total scattering into individual contributions from the neighboring O and Cl, we observe that the peak at $R = 2.0$ and 1.8 Å corresponds to Mg–Cl and Mg–O bonds, respectively. (Note that the absolute values of peak positions in EXAFS do not correspond directly to atomic separations since they include an additional phase shift due to multiple scattering.)

The other NEXAFS measurement for the EtMgCl-$(Et_2AlCl)_2$/THF electrolyte was conducted by Benmayza et al. in 2013.[12] However, instead of focusing on the bulk properties, their interest was in exploring the electrolyte/electrode interfacial region. Using total fluorescence yield to infer the X-ray absorption cross section, we might expect a penetration depth of the order of $\sim 1$ μm at these X-ray photon energies. By comparing the NEXAFS spectrum for the liquid electrolyte and the solid $[Mg_2Cl_3 \cdot 6THF]^+(AlCl_4)^-$ phase, they
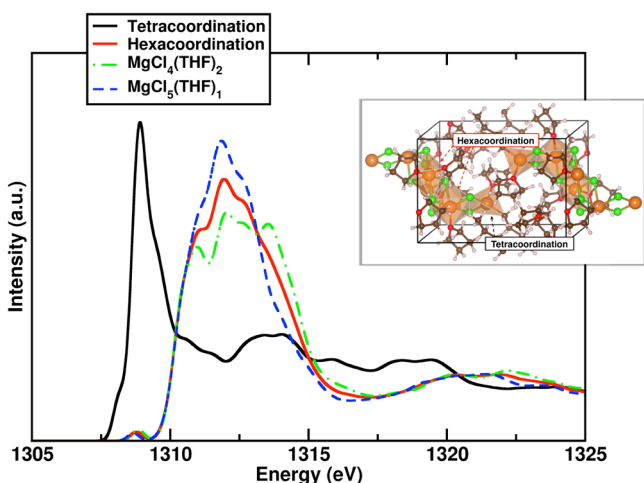


**Figure 8.** Calculated Mg K-edge EXAFS spectra for the $MgCl_2$/THF solution. The black curve is the total scattering for the atoms within 5.5 Å distance from the absorbing Mg atom. The red and green curves indicate the contribution from nearby Cl and O atoms. Inset is the $k^3$ weighted $\chi(k)$ spectrum in $k$ space.

observe similar line-shape and onset energies. Therefore, it is concluded that the hexacoordinated structure should also exist in the liquid electrolyte as identified by the XRD measurement for the recrystallized solid $[Mg_2Cl_3 \cdot 6THF]^+$. Their NEXAFS spectrum shows a main-edge at 1310.5 eV and a broadened shoulder at 1313.5 eV. These results are in good agreement with our simulation for the solid $[Mg_2Cl_3 \cdot 6THF]^+(AlCl_3Et)$ structure although the main-edge and post-edge in our simulation are more distinct. We should note here that in Benmayza's electrolyte sample, the salt concentration is 0.4M, which is close to the solubility limit of $MgCl_2$ in THF solution (0.4–0.7M, depending on the preparation strategy). Comparing these two experimental studies, we propose that at the electrolyte/Mg anode interface, a significant salt concentration gradient exists, or the applied external bias significantly modifies the solvation structure of Mg ions. Exploration of these potential interfacial phenomena warrants further study, both from the theoretical and experimental perspectives.

Recently, Pirinen et al. has successfully prepared a crystalline sample of $MgCl_2$/THF complex that shows the coexistence of tetra- and hexacoordinated Mg.[29] Here we use this structure to further validate our hypothesis that changing from tetracoordination to hexacoordination will shift the onset of the Mg K-

14462

dx.doi.org/10.1021/ja505967u | *J. Am. Chem. Soc.* 2014, 136, 14456–14464

edge NEXAFS spectrum to higher energies. The crystal structure, given in the inset of Figure 9, was first equilibrated



**Figure 9.** Calculated Mg K-edge NEXAFS spectra for $[Mg_3Cl_5(THF)_4C_4H_9]_2$ crystal. Inset is the equilibrated $[Mg_3Cl_5(THF)_4C_4H_9]_2$ crystal structure at 300 K. The shaded area represents the tetra- and hexacoordinated Mg subunits.

at 300 K, and we found that both the tetra- and hexacoordinated Mg subunits are very stable. When performing the NEXAFS simulations on this equilibrated structure, we again obtain distinct K-edge spectra for the tetra- and hexacoordinated Mg atoms. For the tetracoordinated case, Mg is coordinated by two $Cl^-$, one THF, and one $-C_4H_9$ (butyl) group. Compared to the $MgCl_2 \cdot 2THF$ structure, the main edge is red-shifted by ∼1 eV, which is likely a result of the chemical bond to the butyl group. For the hexacoordinated case, the main peak is much more diffuse due to the contribution from two subunits, $MgCl_5(THF)_1$ and $MgCl_4(THF)_2$. In Figure 9, the partial contributions of these two subunits are represented by the dashed lines. For the Mg atom that is coordinated with less THF, i.e. $MgCl_5(THF)_1$, the main peak is well-defined and centered at 1311.9 eV. Increasing the number of THFs broadens the main peak, which is mainly due to the Mg−Cl bond length change within the octahedral cage. Despite the subtle structural difference compared to the $[Mg_2Cl_3 \cdot 6THF]^+(AlCl_3Et)$ structure, the same trend is observed that the hexacoordinated Mg leads to a blue shift of the Mg K-edge NEXAFS spectra.

In general, the structure of $MgCl_2$ in THF solution can be rather complex depending on concentration and local chemical environment. For example, species such as linear polymeric $MgCl_2(THF)_2$, molecular crystal-like $MgCl_2(THF)_2$ and $MgCl_2(THF)_{1.5}$ may all survive in the solution under thermodynamic equilibrium conditions.[34] In this study, we have demonstrated that different solvation structures of Mg can definitely lead to a noticeable change of the NEXAFS spectrum that should be experimentally detectable as both a shift in absolute absorption energy and a change in spectral line shape. However, in our theoretical simulations, we only consider contributions from specific molecular species and solvation structures, while, in reality, measured spectra may comprise contributions from some combination of different species and their associated solvation geometries. In fact, there is a pressing need to deduce or extract the speciation of Mg-ion electrolytes in the bulk or at interfaces and under varying electrochemical

conditions in order to better understand and control the molecular scale mechanisms of electrochemical reactions. If XAS experiments are well-designed with sufficiently high-energy resolution and well-calibrated absolute photon energies to explore samples with diverse speciation, we propose that our simulated spectra and those of future simulations can be used as standard reference spectra, in combination with solvation free-energy estimates, to quantitatively determine that speciation.

## ■ CONCLUSION

The solvation structure of Mg ions in DCC solutions is examined using first-principles methods based on DFT (PBE-GGA). The cluster formation energies in the absence of finite temperature effects for Mg ions interacting with Cl anions and THF molecules are calculated for both monomers and dimers. Based on these gas-phase simulations, the cluster formation energy can easily exceed 2 eV even for the charge neutral species, such as $MgCl_2$ and $Mg_2Cl_4$. For the positively charged species, e.g. $MgCl^+$ and $Mg_2Cl_3^+$, the formation energy can be doubled or tripled. With this information, one can imagine the difficulties to strip THF ligands away from the Mg dication as it approaches the electrolyte/electrode interfaces and wonder at the role of the electrode bias in reducing this likely contribution to the observed over potential.

At finite temperature, we find that the Mg ion favors a tetrahedral coordination, and in the dimer structures, 5-fold coordination is occasionally observed. Based on our energetic analysis at 0 K, the formation energy for the 4- and 5-fold coordination structures differ by little more than the thermal energy at room temperature, which implies that both structures might coexist in the electrolyte under thermodynamic equilibrium.

In this work, within the dilute concentration of $MgCl_2$ in the electrolyte, the Mg ion never forms a hexacoordinated structure, even at 0 K. The appearance of tetracoordination is further confirmed by comparing our calculated Mg K-edge XAS spectrum with a previous experimental study.[7] However, in solid phases, the hexacoordination structure can be stabilized, and the corresponding Mg K-edge NEXAFS spectrum for a recrystallized electrolyte shows a clear blue shift of the main-edge energy. We propose that under typical battery operating conditions, a significant $MgCl_2$ concentration gradient or local fluctuations may exist across the electrode/electrolyte interfacial region. In particular, if the Mg dissolution/deposition kinetics is slow at the interface, higher salt concentrations may appear leading to the growth of oligomers or crystal-like precipitates at the interface. This could be the reason why the Mg K-edge NEXAFS spectra of a DCC solution within ∼1 $\mu m$ of an electrode surface resembles that of hexacoordinated Mg, as measured in the $[Mg_2Cl_3 \cdot 6THF]^+(AlCl_4)^-$ solid phase.[12] In addition, the Mg solvation structure may also be revised by constant bias such as during the charging/discharging cycles. Nevertheless, we have demonstrated in this paper that the core-level excitations of Mg are very sensitive to local solvation structure and coordination. Well-designed *in situ* NEXAFS spectroscopy measurements with high-energy resolution can be performed to track changes in the solvation structure around the Mg ion as it approaches the electrolyte/electrode interface and will provide invaluable insight into the Mg dissolution/deposition mechanism.

## ■ ASSOCIATED CONTENT

### **S** Supporting Information

Examination of the impact of van der Waals interactions on determining the solvation structure of Mg ion. Simulation of $MgCl_2$/THF solvation structures using different theoretical methods. Comparison of the experimental XRD-determined and MD-simulated $[Mg_2Cl_3 \cdot 6THF]^+(AlCl_3Et)$ crystal structures. This material is available free of charge via the Internet at http://pubs.acs.org.

## ■ AUTHOR INFORMATION

**Corresponding Author**
LWan@lbl.gov
**Notes**
The authors declare no competing financial interest.

## ■ ACKNOWLEDGMENTS

## ■ REFERENCES

(1) Yoo, H. D.; Shterenberg, I.; Gofer, Y.; Gershinsky, G.; Pour, N.; Aurbach, D. *Energy Environ. Sci.* **2013**, *6*, 2265.

(2) Liang, Y.; Feng, R.; Yang, S.; Ma, H.; Liang, J.; Chen, J. *Adv. Mater.* **2011**, *23*, 640.

(3) Mitelman, A.; Levi, M. D.; Lancry, E.; Levi, E.; Aurbach, D. *Chem. Commun.* **2007**, 4212.

(4) Levi, E.; Gofer, Y.; Aurbach, D. *Chem. Mater.* **2010**, *22*, 860.

(5) Wang, Z.; Su, Q.; Deng, H. *Phys. Chem. Chem. Phys.* **2013**, *15*, 8705.

(6) Aurbach, D.; Lu, Z.; Schechter, A.; Gofer, Y.; Gizbar, H.; Turgeman, R.; Cohen, Y.; Moshkovich, M.; Levi, E. *Nature* **2000**, *407*, 724.

(7) Nakayama, Y.; Kudo, Y.; Oki, H.; Yamamoto, K.; Kitajima, Y.; Noda, K. *J. Electrochem. Soc.* **2008**, *155*, A754.

(8) Vestfried, Y.; Chusid, O.; Goffer, Y.; Aped, P.; Aurbach, D. *Organometallics* **2007**, *26*, 3130.

(9) Amalraj, S. F.; Aurbach, D. *J. Solid State Electrochem.* **2011**, *15*, 877.

(10) Pour, N.; Gofer, Y.; Major, D. F.; Aurbach, D. *J. Am. Chem. Soc.* **2011**, *133*, 6270.

(11) Gizbar, H.; Vestfried, Y.; Chusid, O.; Gofer, Y.; Gottlieb, H. E.; Marks, V.; Aurbach, D. *Organometallics* **2004**, *23*, 3826.

(12) Benmayza, A.; Ramanathan, M.; Arthur, T. S.; Matsui, M.; Mizuno, F.; Guo, P.; Glans, J.; Prakash, J. *J. Phys. Chem. C* **2013**, *117*, 26881.

(13) Pascal, T. A.; Boesenberg, U.; Kostecki, R.; Richardson, T. J.; Weng, T.-C.; Sokaras, D.; Nordlund, D.; McDermott, E.; Moewes, A.; Cabana, J.; Prendergast, D. *J. Chem. Phys.* **2014**, *140*, 034107.

(14) Merkling, P. J.; Munoz-Paez, A.; Pappalardo, R. R.; Marcos, E. S. *Phys. Rev. B* **2001**, *64*, 092201.

(15) Jalilehvand, F.; Spangberg, D.; Lindqvist-Reis, P.; Hermansson, K.; Persson, I.; Sandstrom, M. *J. Am. Chem. Soc.* **2001**, *123*, 431.

(16) Kohn, W.; Sham, L. J. *Phys. Rev.* **1965**, *140*, A1133.

(17) Kresse, G.; Furthmuller. *Comput. Mater. Sci.* **1996**, *6*, 15.

(18) Kresse, G.; Hafner, J. *Phys. Rev. B* **1993**, *47*, 558.

(19) Perdew, J. P.; Burke, K.; Ernzerhof, M. *Phys. Rev. Lett.* **1996**, *77*, 3865.

(20) Blochl, P. E. *Phys. Rev. B* **1994**, *50*, 17953.

(21) Kresse, G.; Joubert, D. *Phys. Rev. B* **1999**, *59*, 1758.

(22) Nose, S. *J. Chem. Phys.* **1984**, *81*, 511.

(23) Giannozzi, P.; et al. *J. Phys.: Condens. Matter.* **2009**, *21*, 395502.

(24) Prendergast, D.; Louie, S. G. *Phys. Rev. B* **2009**, *80*, 235126.

(25) Vanderbilt, D. *Phys. Rev. B* **1990**, *41*, 7892.

(26) Prendergast, D.; Galli, G. *Phys. Rev. Lett.* **2006**, *96*, 215502.

(27) England, A. H.; Duffin, A. M.; Schwartz, C. P.; Uejio, J. S.; Prendergast, D.; Saykally, R. J. *Chem. Phys. Lett.* **2011**, *514*, 187.

(28) Ankudinov, A. L.; Ravel, B.; Rehr, J. J.; Conradson, S. D. *Phys. Rev. B* **1998**, *58*, 7565.

(29) Pirinen, S.; Koshevoy, I. O.; Denifl, P.; Pakkanen, T. T. *Organometallics* **2013**, *32*, 4208.

(30) Gigli, G. *J. Chem. Phys.* **1990**, *93*, 5224.

(31) Drisdell, W. S.; Poloni, R.; McDonald, T. M.; Long, J. R.; Smit, R.; Neaton, J. B.; Prendergast, D.; Kortright, J. B. *J. Am. Chem. Soc.* **2013**, *139*, 035104.

(32) Lindner, T.; Sauer, H.; Engel, W.; Kambe, K. *Phys. Rev. B* **1986**, *33*, 22.

(33) Nakanishi, K.; Ohta, T. *J. Phys.: Condens. Matter* **2009**, *21*, 104214.

(34) Sobota, P. *Chem.—Eur. J.* **2003**, *9*, 4854.